THE ASTROPHYSICAL JOURNAL 251:162–180, 1981 December 1

OUTER ATMOSPHERES OF COOL STARS. VIII. *IUE* OBSERVATIONS AND CHROMOSPHERIC MODELS FOR THE SUPERGIANT STARS β DRACONIS, ϵ GEMINORUM, AND α ORIONIS

GIBOR S. BASRI,[1, 2] JEFFREY L. LINSKY,[1, 3] AND KJELL ERIKSSON
Joint Institute for Laboratory Astrophysics, National Bureau of Standards and University of Colorado
Received 1980 August 21; accepted 1981 January 19

ABSTRACT

We extend our program of semiempirical modeling of stellar chromospheres to a previously unstudied portion of the H-R diagram—the late-type supergiants. These models were computed to match high-resolution absolute flux profiles of the Ca II K and Mg II *h* and *k* lines. In our *IUE* ultraviolet spectra of ϵ Gem and α Ori we find no evidence for emission lines formed at temperatures hotter than $\sim 10^4$ K, and on this basis we compute chromospheric models which extend to $m = 10^{-6}$ g cm^{-2} at temperatures rising to 6500 K and 7000 K, respectively. Upper limits on the surface flux of the C IV λ1549 emission feature in ϵ Gem are 0.1 that of the quiet Sun, and in α Ori the upper limits are 0.002 that of the quiet Sun, providing upper limits on the amount of 10^5 K plasma in these stars. By contrast, β Dra shows strong emission lines of C II–IV, Si IV, He II, and N V. We tentatively extend the β Dra chromospheric model up to 16,000 K at $P_0 = 2n_e kT = 0.012$ dynes cm^{-2}. However, density-sensitive line ratios suggest $P_0 = 0.3$ dynes cm^{-2} at 60,000 K, and we discuss possible explanations for the discrepancy.

Chromospheric models for supergiants are more uncertain than for giants and dwarfs because low stellar gravity results in low chromospheric densities and thus highly coherent scattering in the wings of the Ca II and Mg II resonance lines. We take this coherency into account in our partial redistribution (PRD) code, but it results in the line wings being insensitive to local atmospheric parameters at the base of the chromosphere. The highly asymmetric line profiles for β Dra are modeled with a comoving PRD code which assumes a sinusoidal variation of vertical velocity amplitude with positive (outward) velocity maximum near the temperature minimum and negative (inward) velocity maximum near $m = 10^{-2}$ g cm^{-2} (near $\tau_K \approx 1$). This velocity structure is ad hoc, but it is qualitatively consistent with a circulation pattern like solar supergranulation in which bright regions (network) are downflows and dark regions (cells) are upflows. We discuss alternative explanations. Finally, we point out that our analyses of the Ca II and Mg II lines, assuming hydrostatic equilibrium with only thermal and turbulent components to the pressure, imply nearly plane-parallel chromospheres, even for α Ori. Since other data suggest considerable geometrical extent for the chromospheres of α Ori and other *M* supergiants, future models should include geometrical extension when estimates of nonthermal components of the pressure become available.

Subject headings: stars: chromospheres — stars: late-type — stars: supergiants — ultraviolet: spectra

I. INTRODUCTION

In the last several years major progress has been achieved toward the goal of determining the physical characteristics of chromospheres in different regions of the Hertzsprung-Russell (H-R) diagram. One approach is to derive semiempirical chromospheric models of the temperature, density, and velocity distributions by matching non-LTE partial redistribution (PRD) calculations with observed profiles of strong resonance lines, primarily those of Ca II and Mg II. Linsky (1980*a*, *b*) has reviewed this effort which to date has included main-sequence stars of spectral type F–K and giants of spectral type G and K. A complementary approach is to assume a nonradiative heating mechanism and to derive theoretical models that can be compared with semiempirical models of individual stars. This approach has been reviewed most recently by Ulmschneider (1979) and by Linsky (1980*a*, *b*). Linsky (1981) has reviewed the evidence for chromospheres, coronae, and wings in late-type stars.

The purpose of this paper is to extend the semiempirical modeling approach to a previously unstudied portion of the H-R diagram—the late-type supergiants. Because these stars have very low gravity atmospheres, they present an opportunity to study partial redistribution diagnostics under conditions of nearly complete coherency and, more importantly, to assess the gravity

[1] Guest Observer with the *International Ultraviolet Explorer* (*IUE*) satellite.
[2] Now at the Space Science Laboratory, University of California, Berkeley.
[3] Staff Member, Quantum Physics Division, National Bureau of Standards.

dependence of chromospheric properties, such as nonradiative heating rates and velocity fields.

There are four natural parameters that can be used to characterize chromospheric temperature distributions. Taking the mass column density as the basic depth variable, they are: $T_{\rm min}$ (the minimum temperature); $m(T_{\rm min})$; $dT/d\log m$ in the chromosphere, if for simplicity we take the temperature distribution as linear in $\log m$; and m_0, the mass column density at the base of the transition region. For quiet chromosphere stars, Kelch *et al.* (1978) found that $T_{\rm min}$ is roughly proportional to $T_{\rm eff}$, and Ayres (1979) has argued on theoretical grounds that $m(T_{\rm min}) \sim g^{-1/2}$. A natural consequence of the assumptions used by Kelch *et al.* (1978) in computing chromospheric models is that $m_0 \sim g^{-1/2}$ also, but this result may not be valid in general as the Lyman continuum can be formed at temperatures different from the 8000 K assumed, depending on the temperature gradients in the upper chromosphere (cf. Baliunas *et al.* 1979). In any case, there is some evidence that chromospheres occur at larger values of the mass column density with decreasing stellar gravity. Thus the pressures ($P = mg$) and densities of supergiant chromospheres may be smaller than for dwarfs, perhaps by a factor of $g^{1/2}$ instead of by a factor of g.

These trends, which appear to be valid for quiet chromosphere stars but not active chromosphere stars (cf. Baliunas *et al.* 1979), tend to be masked by the great range in emission-line strength (often called chromospheric activity) seen in stars of similar spectral type. Since these emission lines provide most of the cooling in the upper chromosphere, their increase in strength per unit area of the star is generally interpreted as an increase in the chromospheric nonradiative heating rate, $F_{\rm NR}$. Models for these active chromospheres have larger values of $dT/d\log m$, m_0, and $T_{\rm min}$ than similar quiet models (cf. Kelch, Linsky, and Worden 1979; Baliunas *et al.* 1979). Qualitatively, the differences are similar to those between quiet Sun and plage models (Shine and Linsky 1974; Kelch and Linsky 1978) and between dark cell centers and very bright network elements (Vernazza, Avrett and Loeser 1981). Thus the four chromospheric temperature distribution parameters are likely determined by the chromospheric nonradiative heating rate, $F_{\rm NR}$, in addition to the stellar gravity. Since magnetic fields play an important role in defining active versus quiet regions on the Sun, active chromosphere stars probably have larger fractions of their stellar surface covered by strong magnetic fields.

One of the biggest problems with the semiempirical modeling approach is that one has sufficient data to compute only a one-component model, but we know from the solar example that chromospheres can be very inhomogeneous. It is not clear what relation a single-component model atmosphere derived from a stellar line flux has to the many different components likely to coexist on the stellar surface. Hot components, perhaps magnetic flux tubes, probably coexist with cooler regions, and the activity range we observe may be simply a reflection of the different proportions of these two components that exist on different stars. Thus the properties of a single-component model may not accurately portray the conditions in any of the components actually present in the atmosphere, but instead they may represent an average of these components weighted in a complex way. Nevertheless, at this early stage in the study of stellar chromospheres, it is important to compare single-component models of various stars with each other if only to obtain a rough estimate of the relative importance of the hot components in different stars.

II. OBSERVATIONS

The data used for modeling in this work consist of high-resolution profiles, calibrated in absolute flux units, of the Ca II K line (3933 Å) and Mg II *k* line (2796 Å), and calibrated low-resolution ultraviolet spectra in the region 1150–2000 Å. The high-resolution K-line data (Fig. 1) are taken from Linsky *et al.* (1979*b*) and the Mg II data (Fig. 1) from Basri and Linsky (1979). The low-resolution ultraviolet spectra (Fig. 2) were obtained using the *International Ultraviolet Explorer* (*IUE*) satellite (cf. Boggess *et al.* 1978; Linsky *et al.* 1978). These data have a resolution of ~ 6 Å, sufficient to determine fluxes in strong lines. The large-aperture *IUE* spectra were calibrated using the factors determined by Turnrose, Bohlin, and Harvel (1980) and Cassatella *et al.* (1980). Table 1 summarizes the *IUE* observations.

a) β Draconis (G2 II)

The Ca II and Mg II profiles for this star are characterized by a blue asymmetry (shortward wavelength-emission peak brighter than longward peak), which is far more pronounced in Ca II than Mg II, and a rather surprising emission width, implying a very large Wilson-Bappu magnitude of $M_V = -5.2$. The parallax of the star, given as 0.009 in the *Bright Star Catalog*, is very uncertain, but it implies that $M_V = -2.5$, which seems a more reasonable value for a luminosity class II star. Wilson and Bappu (1957) list the Yerkes magnitude as -2. The K line does not show the deep central reversal present in the other two supergiants. The depth of the broad Mg II resonance feature is much less than for a dwarf of a similar spectral type; that is, the slope of the line wings is much shallower. The surface fluxes and thus the amount of radiative cooling in these lines are large compared with G–K giants and supergiants (cf. Linsky *et al.* 1979*b*; Basri and Linsky 1979).

The far-ultraviolet spectrum (see Fig. 2) shows high-temperature emission lines typical of the solar transition region, including C II, III, IV, Si IV, He II, and N V, as well as chromospheric emission lines of C I, O I, S I, and Si II. A list of identified lines and their observed fluxes and estimated surface fluxes appears in Table 2. Line identifications were made using the solar limb and flare line lists of Burton and Ridgeley (1970) and Cohen, Feldman, and Doschek (1978). We note that the intersystem lines of N IV (λ1487), Si III (λ1892), C III (λ1909), and especially N III ($\lambda\lambda$1750, 1754) are more prominent in the spectrum of β Dra than in less luminous stars of similar effective temperature like the Sun (G2 V) and

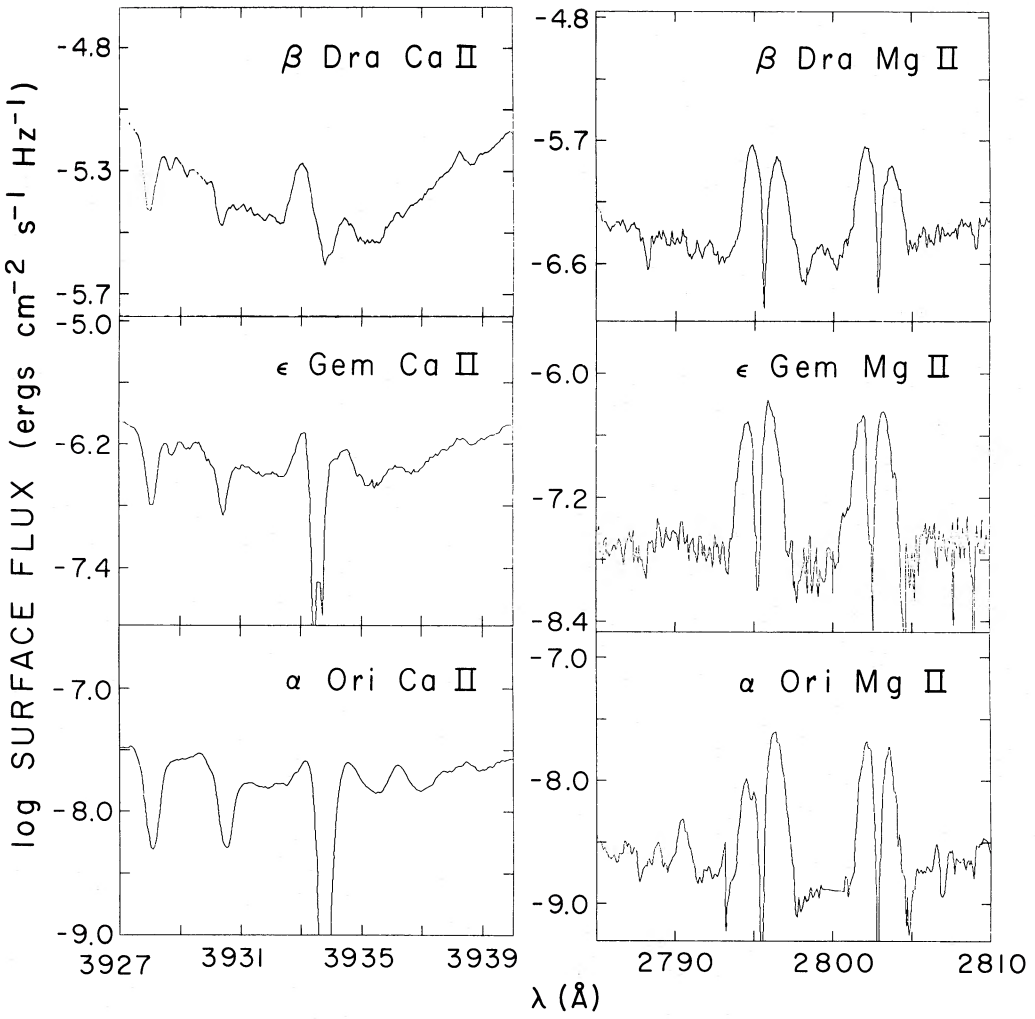

FIG. 1.—Ca II K line profiles in absolute flux units taken from Linsky *et al.* (1979*b*) and Mg II *h* and *k* line profiles in absolute flux units taken from Basri and Linsky (1979).

TABLE 1

SUMMARY OF *IUE* LOW DISPERSION OBSERVATIONS

Star	Spectral Type	*IUE* Image	Effective Exp. Time (min)[a]	Aperture[b]	Date
β Dra	G2 II	SWP 2348	24	L	1978 Aug 21
		SWP 2349	60	L	1978 Aug 21
		SWP 2350	10	L	1978 Aug 21
ε Gem.....	G8 Ib	SWP 2337	48	L	1978 Aug 19
α Ori	M2 Iab	SWP 1311	8	S	1978 Apr 4
		SWP 1312	72	S	1978 Apr 4
		SWP 2322	90	L	1978 Aug 17

[a] Comparison of relative fluxes in SWP 2322 with the small aperture images (SWP 1311, 1312) implies an effective transmission of 40% for the small aperture at this time. The small aperture effective exposure times are therefore 0.40 times the clock exposure times.

[b] S = 3″ diameter small aperture; L = 10″ × 20″ large aperture.

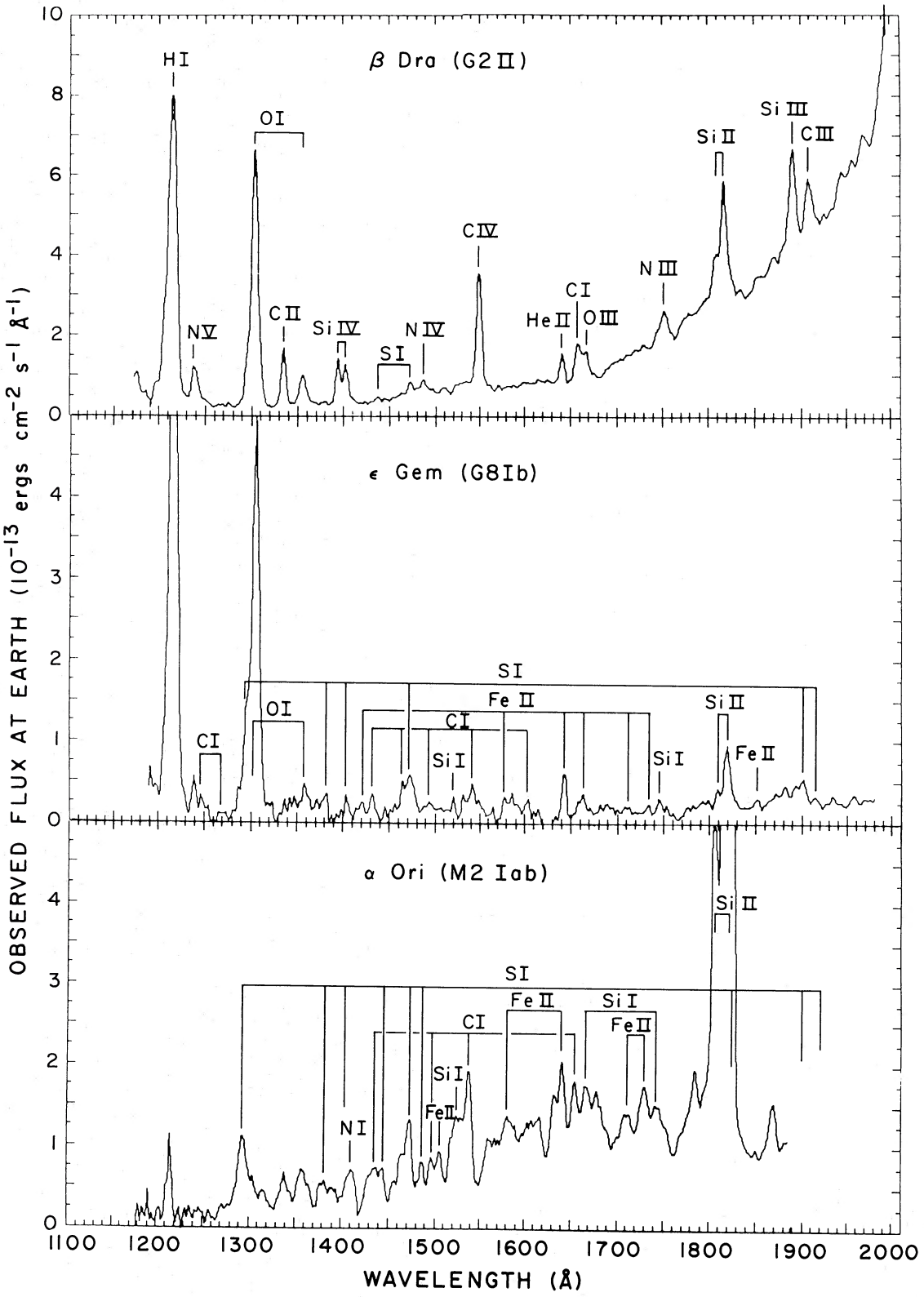

FIG. 2.—*IUE* low dispersion spectra in absolute flux units. Prominent emission lines are identified. The Lyα emission lines are mostly geocoronal in origin.

TABLE 2

LINE IDENTIFICATIONS AND FLUXES FOR β DRACONIS[a]

Wavelength (Å)	Probable Identification[b]	Observed Flux (ergs cm^{-2} s^{-1})	Surface Flux[c] (ergs cm^{-2} s^{-1})	Surface Flux[d] / Quiet Sun
1176	C III (4)	7.5(−13)	1.2(4)	7.5
1215	Lα[e]	...	...	...
1239	N V (1)	7.8(−13)	1.2(4)	14
1304	O I (2), Si III (4)	6.4(−12)	1.0(5)	25
1335	C II (1)	9.5(−13)	1.5(4)	3.3
1355	O I (1)	7.5(−13)	1.2(4)	35
1394	Si IV (1)	7.5(−13)	1.2(4)	7.1
1402	Si IV (1), O IV	8.1(−13)	1.3(4)	17
1438	S I (5)	...	...	...
1473	S I (4), S I (3)	1.6(−13):	2.5(3):	4.8:
1487	N IV, S I (4)	1.4(−13):	2.3(3):	...
1509	C I, N II (6)?	1.7(−13):	2.7(3):	...
1549	C IV (1)	2.4(−12)	3.8(4)	6.6
1641	He II (12), Fe II (42, 43)	4.8(−13)	7.6(3)	5.8
1658	C I (2)	8.5(−13)	1.4(4)	2.6
1666	O III	5.4(−13)	8.5(3)	...
1712	Fe II (38), Si I?	...	...	...
1720	Fe II (38)	...	...	...
1729	Fe?, Si I?	...	...	...
1752	N III (19 UV)	1.1(−12)	1.7(4)	...
1777	...	...	...	...
1809	Si II (1)	8.3(−13)	1.3(4)	2.1
1818	Si II (1)	2.7(−12)	4.3(4)	4.3
1835	Fe II (98)	1.9(−13):	3.0(3):	...
1855	Al III (1)	2.2(−13):	3.5(3):	...
1871	...	2.7(−13):	4.3(3):	...
1891	Si III (1)	1.7(−12)	2.7(4)	...
1908	C III	1.1(−12)	1.7(4)	...
1925	Fe II (123)?	...	...	...
1945	...	3.1(−13):	4.9(3):	...
1957	...	1.8(−13):	2.9(3):	...
1969	...	4.2(−13)	6.7(3)	...

[a] Composite of images SWP 2348, 2349, and 2350.
[b] Probable prime contributor is listed first. Multiplet number is in parenthesis.
[c] Flux per unit area at the surface of the star assuming an angular diameter of 3.27 milli-arcsec.
[d] Quiet Sun surface fluxes from Linsky *et al.* 1978.
[e] Major component is probably geocoronal emission.

Capella (G6 III+F9 III) (cf. Ayres and Linsky 1980). Surface fluxes were estimated using the Barnes-Evans relations (see eqs. [1] and [2] in Linsky *et al.* 1979*b*). The surface fluxes in these lines lie in the range of 2–35 times those in the quiet Sun, which implies a stronger source of nonradiative heating than in the quiet Sun. It will be of great interest to obtain high-resolution profiles of some of the brighter transition region lines to see if they are as broad as implied by the Wilson-Bappu relation.

b) ϵ *Geminorum* (*G8 Ib*)

An interesting feature of the Ca II resonance lines in this star (see Fig. 1) is the appearance of several distinct absorption components in the core, which are presumably circumstellar in origin and make it difficult to assess the intrinsic chromospheric emission-line profile. In addition to a zero velocity feature with very small residual intensity, which could be both interstellar and circumstellar in origin, there is both a blueshifted and a redshifted component. The red component was much shallower than the others in 1976 and seemed to have disappeared in 1978 (Chiu, private communication). These features likely represent absorption by an inhomogeneous circumstellar shell around the star. Unfortunately, the resolution of the Mg II data is too low to measure these components, but these data do allow a measurement of the peak fluxes in the chromospheric profile. The Ca II profile is too mutilated by absorption to show line-profile asymmetries; the Mg II data suggest a slight redward asymmetry. The wings of the *k* line are likely underexposed in our data, but are apparently flat in contrast to the K-line wings.

The 1150–2000 Å *IUE* spectrum (Fig. 2) shows no evidence for the strong-transition region lines (i.e., C IV, Si IV, He II, and C II) prominently seen in the spectrum of β Dra. There are weak features at the location of the C III λ1175 and N V λ1240 lines, but, in view of the absence of transition region lines which are typically stronger than λ1175 and λ1240, we conclude that C III and N V are not present. Although a longer exposure should be made of ϵ Gem, we believe on the basis of our spectrum that there is little if any material hotter than 10,000 K in the outer

TABLE 3

LINE IDENTIFICATIONS AND FLUXES FOR ϵ GEMINORUM AND α ORIONIS[a]

WAVELENGTH (Å)		PROBABLE IDENT.[b]	OBSERVED FLUX[c]		SURFACE FLUX[d]	
ϵ Gem	α Ori		ϵ Gem	α Ori	ϵ Gem	α Ori
1215	1216.....	H I[e]	...	...	...	...
...	1235.....	...	...	...	...	...
1239	... .	N V??, Fe II?	2.5(−13)	...	1.6(3)	...
1246	1247.....	C I	1.5(−13):	...	9.5(2):	...
...	1258.....	Si I				
1270	... .	C I	1.1(−13):	...	7.2(2):	...
...	1296.....	S I	...	1.4(−12)	...	8.1(1)
1305	... .	O I, S I	5.8(−12)	...	3.7(4)	...
...	1318.....	S I?, N I?	...	2.6(−13)	...	1.5(1)
...	1340.....	CO	...	3.6(−13)	...	2.1(1)
1358	1358.....	O I (1)	2.6(−13)	5.5(−13)	1.6(3)	3.2(1)
1381	1383.....	CO	...	2.7(−13)	...	1.6(1)
1403	... .	S I?	1.1(−13):	...	7.0(2):	...
...	1412.....	CO, N I?	...	5.8(−13)	...	3.4(1)
1421	... .	Fe II?	1.4(−13):	...	8.8(2):	...
1432	1433.....	C I (65), S I (5)	1.8(−13)	} 9.3(−13)	1.1(3)	} 5.4(1)
...	1444.....	S I	...		...	
1464	... .	C I (37)	} 6.1(−13)	...	} 3.9(3)	...
1473	1474.....	S I (4, 3)		9.0(−13)		5.2(1)
...	1487.....	S I	...	1.7(−13):	...	1.0(1):
1493	... .	C I	1.2(−13)	...	7.6(2)	...
...	1497.....	CO	...	2.3(−13)	...	1.3(1)
...	1508.....	Fe II	...	3.5(−13)	...	2.0(1)
1520	1523.....	Si I	...	} 2.5(−12)	...	} 1.5(2)
1541	1540.....	C I, Fe II, CO	5.0(−13)		3.2(3)	
1549[f]	1549[f]	C IV (1)	<8(−14)	<1.5(−13)	<5(2)	<9(0)
...	1569.....	Si I, Fe II	...	...	...	...
1579	1580.....	Fe II (44)	} 3.4(−13)	} 9.9(−13)	} 2.1(3)	} 5.8(1)
1586	... .	Si II				
1603	... .	C I (63), CO?	1.4(−13):	...	8.8(2):	...
1644	1642.....	Fe II (42)	3.3(−13)	1.4(−12)	2.1(3)	8.1(1)
...	1656.....	C I (2)	...	7.4(−13)	...	4.3(1)
1662	... .	Fe II	2.3(−13)	...	1.5(3)	...
...	1669.....	Si I, Fe II	...	8.2(−13)	...	4.8(1)
1711	1712.....	Fe II, CO?	8.9(−14):	5.1(−13)	5.6(2):	3.0(1)
1733	1732.....	Fe II	7.4(−14):	8.3(−13)	4.7(2):	4.8(1)
1745	1745.....	Si I (79), Fe II	1.6(−13)	7.1(−13)	1.0(3)	4.1(1)
...	1785.....	...	...	1.2(−12)	...	7.0(1)
1809	1809.....	Si II	} 8.9(−13)	3.8(−12)	} 5.6(3)	2.2(2)
1819	1822.....	Si II, S I, Fe II		1.0(−11)		5.8(2)
1852	1850.....	Fe II (65)	1.0(−13)	...	6.3(2)	...
...	1871.....	...	...	5.3(−13)	...	3.1(1)
1901	1900.....	S I (1)	5.1(−13)	SAT	3.2(3)	...
1915	1916.....	S I (1)	1.3(−13)	SAT	8.2(2)	...
1934	... .	Fe II	...	...	...	...
...	1942.....	...	...	...	...	...
1958	1957.....	...	1.2(−13)	...	7.6(2)	...

[a] Composite of images SWP 1311, 1312, and 2322.
[b] Probable prime contributor is listed first. Multiplet number is in parenthesis.
[c] Flux observed by *IUE* in ergs cm^{-2} s^{-1}.
[d] Flux per unit area at the surface of the star assuming angular diameters of 5.19 milli-arcsec for ϵ Gem and 54.08 milli-arcsec for α Ori. Units are ergs cm^{-2} s^{-1}.
[e] Major component is probably geocoronal emission.
[f] 3 σ upper limit.

atmosphere of this star. The spectrum is characterized by strong O I emission and by emission lines of Fe II, Si II, Si I, C I, and S I (see Table 3). The O I resonance lines are likely pumped by H I Lyβ as discussed by Haisch *et al.* (1977) for Arcturus. Identifications are often difficult and ambiguous at this resolution, but the important information in the spectrum is the absence or great weakness of transition-region emission lines and the prominent low-temperature emission lines. For example, we estimate a 3 σ upper limit on the strength of the C IV λ1549 feature of 8×10^{-14} ergs cm^{-2} s^{-1}, corresponding to a surface flux of 50 ergs cm^{-2} s^{-1} or about 0.1 that of the quiet Sun. Since the Mg II *h* and *k* lines in ϵ Gem have a surface flux ≈ 0.4 that of the quiet Sun (Basri and Linsky 1979), the C IV upper limit implies at least a factor of 4 decrease in the amount of 10^5 K plasma compared to the amount of chromospheric material in ϵ Gem. This apparent absence of weakness of transition-region emission lines appears to be a property of stars to the right of the dividing line in the H-R diagram proposed by Linsky and Haisch (1979). These stars also typically show evidence for outflowing material (redward asymmetry) and/or circumstellar absorption features (cf. Stencel 1978; Stencel and Mullan 1980). Since no transition-region emission lines are visible, we can only model the chromosphere layers where the Ca II and Mg II lines are formed.

c) α *Orionis* (*M2 Iab*)

Both the Ca II and Mg II lines in this star have rather broad, dark central cores and large emission widths appropriate to a star of this luminosity class. The question of whether or not the central absorption cores are due to circumstellar absorption is discussed in § IV*c*. The *k*-line emission peaks are asymmetric as expected due to Fe I and Mn I circumstellar absorption (Bernat and Lambert 1976; de Jager *et al.* 1979), but the *h* line shows an almost symmetric profile. This is surprising since α Ori is known to possess a very extensive circumstellar shell and a fairly high mass loss rate. If the interpretation of redward asymmetry as being indicative of mass loss is valid, then one would expect a large asymmetry in this star.

The far-ultraviolet spectrum of α Ori (see Fig. 2 and Table 3) is a composite of two small-aperture exposures and one large-aperture exposure. The small-aperture spectra were put on an absolute flux scale by comparison with the large-aperture image SWP 2322. This comparison led to the conclusion that the transmission of the small aperture was about 40% and the total effective exposure time was about 90 minutes. In forming the composite image, care was taken in deleting saturated pixels and in properly registering the individual wavelength scales. Essentially all of the strong emission features are present in both of the long exposures (SWP 1312 and 2322).

The α Ori spectrum is similar to that of ϵ Gem in that there is no evidence for emission at the wavelengths of prominent high-temperature lines such as those of C II, C IV, Si IV, and N V. Since the composite α Ori image is deeply exposed, we feel confident in saying that the amount of high-temperature plasma must be very small. For example, a reasonable 3 σ upper limit on the strength of the C IV λ1549 feature is about 1.5×10^{-13} ergs cm^{-2} s^{-1}, corresponding to a surface flux of 9 ergs cm^{-2} s^{-1} or about 2×10^{-3} that of the quiet Sun. Since the Mg II *h* and *k* lines have a surface flux of 0.02 that of the quiet Sun (Basri and Linsky 1979), the C IV upper limit implies at least a factor of 10 decrease in the amount of 10^5 plasma compared to the amount of chromospheric material in α Ori. The spectrum of α Ori does differ from that of ϵ Gem in three important ways. First, the O I λ1304 resonance triplet is very weak or absent, implying weak hydrogen Lyman emission (and thus no pumping by Lyβ) or attenuation by interstellar oxygen. Second, the S I spectrum is very strong. It is the dominant contributor to the λ1296 feature, the λ1820 blend with Si II, and the λ1901 and λ1916 lines are saturated (not plotted in Fig. 3). Carpenter and Wing (1979) have shown that S I dominates the λ1820 feature in their high-resolution spectrum of α Ori. Third, emission features at λ1340, λ1383, λ1412, and at longer wavelengths are likely due to fluorescence of CO fourth positive bands pumped by resonance lines of H I, O I, and C I (Ayres, Moos, and Linsky 1981). Weak CO features may be present in the ϵ Gem spectrum at longer wavelengths.

d) *Comparison with the Spectra of* α *Aquarii* (*G2 Ib*) *and* β *Aquarii* (*G0 Ib*)

Hartmann, Dupree, and Raymond (1980) have pointed out that α Aqr and β Aqr show blueshifted absorption features in the Mg II lines at velocities up to 126 km s^{-1}, indicative of high-velocity cool winds, and emission lines of C IV and N V, indicative of plasma at least as hot as 200,000 K. On the basis of the identification in these stars of both a cool wind and hot plasma, they designate these stars as "hybrid." β Dra lies just below α Aqr and β Aqr in the H-R diagram and has a rather similar far-ultraviolet spectrum in appearance. One difference is that the β Dra surface fluxes are an average of 3.6 times those of α Aqr and 5.0 times those of β Aqr, relatively independent of the temperature of ion formation. However, the Mg II and Ca II profiles have very different asymmetries in that the β Dra profiles show no evidence for a wind, but rather they suggest mass infall or a circulation pattern in which the bright patches on the surface are systematically moving downward (see § IV*a*). By comparison, α Aqr and β Aqr show clear evidence of mass outflow in the Mg II lines.

The supergiant ϵ Gem has a luminosity similar to α Aqr and β Aqr, but it has a somewhat lower effective temperature. ϵ Gem shows evidence for mass loss (blueshifted circumstellar absorption in the K line and red emission peaks brighter than blue emission peaks in the Mg II lines) similar to α Aqr and β Aqr, but ϵ Gem shows no evidence for high-temperature emission lines. In short, ϵ Gem lies clearly to the right of the Linsky-Haisch dividing line in the H-R diagram.

These two comparisons suggest that the outer atmosphere properties of G stars with luminosity classes II and Ib depend very sensitively on one or more parameters. For example, β Dra and β Aqr may be relatively rapid

rotators for their spectral types, as Uesugi and Fukuda (1970) cite $v \sin i = 13$ and 18 km s^{-1}, respectively. Only upper limits are available for the other two stars. It is possible that β Dra has mainly closed magnetic structures, whereas the more luminous and, thus, lower gravity stars α Aqr and β Aqr have both open and closed magnetic field structures, which result in cool winds and hot (and presumably stationary) components. By comparison, ϵ Gem may have only open fields in its outer atmosphere and thus no hot plasma component. Clearly these questions need to be pursued vigorously. One step in this study is the detailed chromospheric modeling which follows.

III. PROCEDURES FOR COMPUTING SUPERGIANT MODEL CHROMOSPHERES

The atomic parameters used in this work were adopted from Ayres (1975) for H I, Mg II, and Ca II and from Lites, Shine, and Chipman (1978) for C II. As these calculations are exploratory, simple model atoms were chosen. For Ca II we employed a five-level model atom with five explicit transitions, the H and K lines and the infrared triplet lines, $\lambda\lambda$8498, 8542, and 8662. Shine, Milkey, and Mihalas (1975) have shown that this approach yields fairly accurate results in the solar case. Cross-redistributions are taken into account approximately by setting a lower bound to the incoherence due to infrared triplet photons arising in the wings of the upper levels. A five-level atom is also used for Mg II, consisting of the lower and upper levels of the h and k lines and the overlying 3^2D levels. These latter levels are included only because they supply the major redistribution in the h and k lines (Basri 1980). Because the subordinate lines ($3^2D - 3^2P$) actually overlap the red wings of the h and k lines, it is very difficult to treat the radiative transfer in these lines precisely, and we include them approximately to check whether the 3^2D level populations are close to local thermodynamic equilibrium (LTE). Four levels are included in the model C II ion in order to treat the λ1037 and λ1335 resonance lines explicitly and to check redistribution from the level overlying the λ1335 upper state. Hydrogen is treated by including the first five levels, and the Lyman continuum, Lyα, Lyβ, and Hα transitions are treated explicitly as in Basri *et al.* (1979). The primary need for this calculation is to determine the electron density and the departure coefficient in the Balmer continuum, which are important for redistribution in the Mg II line wings. All abundances were assumed to be solar.

The first star chosen for analysis was β Dra because this star is most similar to previously studied cases, such as α Aur (cf. Kelch *et al.* 1978). Fluxes of the C II $\lambda\lambda$1334, 1335 resonance lines are sensitive both to the pressure, $P_0 = m_0 g$, at the base of the transition region and to the thickness of any plateau which might exist near 2×10^4 K (cf. Simon, Kelch, and Linsky 1980; Lites, Shine, and Chipman 1978). For simplicity the lines were assumed to be of equal intensity, as is very nearly the case in the Sun (Lites, Shine, and Chipman 1978). Since the line widths are unknown, we could only try to match the calculated integrated flux to the observed flux. The collisional damping parameters are not known for C II, but the densities in supergiant chromospheres are so low where these lines are formed that the likely major source of redistributions is a cascade from the next higher level. Because C II is not seen in ϵ Gem or α Ori, we assumed that their chromospheres extend outward to very low mass column densities without the temperature rising any more than necessary to explain Ca II and Mg II intensities. Thus there is no defined "top" to the model chromospheres of ϵ Gem or α Ori.

The next step was to adjust the chromospheric temperature structure in order to match the observed Ca II and Mg II line surface flux profiles. These lines together tend to constrain the chromospheric model well because there is good overlap in the contribution functions, except for the inner core of Mg II k which is formed above that of Ca II K. The lines have similar oscillator strengths, so the difference in height of formation results mostly from the difference in abundance and ionization potentials of the two elements. The other major difference is the presence of the intermediate metastable levels in Ca II, which provide an upper bound to the coherence of the K-line wings. For the Mg II resonance lines this upper bound is provided by a higher lying level that is very much less populated relative to the k-line upper level. Thus the incoherence fraction Λ for Ca II K can be no smaller than 0.025, whereas Λ can be as small as 10^{-4}–10^{-6} for Mg II k (Basri 1980). The limiting value for Λ in Ca II is actually 0.06 in LTE, but calculations show that the radiation field in the infrared triplet in the upper chromosphere is typically less than half of its LTE value. Apart from this limit, we used values for Λ calculated for collisional damping using the hydrostatic particle densities with damping parameters found by Ayres (1977).

We generally found that models which fit the K line yield low fluxes in the k line, and that models which fit the k line yield K-line fluxes that are high. It was reasonably straightforward to find models that match observed fluxes at K_2 and k_2, but these models produce narrow-emission features and faint wings in k and bright wings in K. In all cases, the central reversals are very deep. Previous attempts at model chromospheres have been concerned mostly with matching the computed integrated flux between the K_1 or k_1 minimum features with observations, but we are concerned here with trying to reproduce all features of the line profiles to understand the stellar velocity fields and the Wilson-Bappu effect. The models required to fit the Ca II and Mg II line profiles are therefore fairly unique; in fact, the problem was somewhat overconstrained in the sense that we could never quite match the observed fluxes of both the K and k lines with a single model. Given that these data are full disk averages of what are likely very inhomogeneous chromospheres, it is probably not useful at this time to carry the process any further.

Once an initial model chromosphere has been settled on, the next step is to compute radiation temperatures for those transitions that will not be treated explicitly in the

TABLE 4

CHROMOSPHERIC RADIATION TEMPERATURES (K)

Hydrogen Continuum	β Dra	ϵ Gem	α Ori
Balmer	4720	3970	2780
Paschen	4320	3670	2665
Brackett	3910	3370	2480
Pfund	3590	3100	2300

multilevel non-LTE calculations. These transitions are all thinner than the lines of interest, and because the dominant transfer process for those lines is resonant scattering, the level populations are controlled mostly by the background radiation fields and the line opacities. We used a simple absorption-plus-scattering source function to calculate the radiation field at a few frequency points in each continuum, and then integrated over frequency to find the photoionization rates and radiation temperatures in each continuum. The derived chromospheric radiation temperatures for the Balmer and higher continua of hydrogen are given in Table 4. In the photosphere the local radiation temperatures equal their chromospheric values or the local electron temperature, whichever is larger. The assumption of LTE for the absorption source functions in the bound-free continua is unlikely to be valid in supergiant chromospheres. Instead, we used calculated departure coefficients for the hydrogen Lyman and Balmer continua. For hydrogen, rates for those bound-bound transitions that are not explicitly treated were assumed to be in detailed balance throughout the atmosphere.

For all the models computed we have assumed hydrostatic equilibrium, which results in essentially planar geometries. We therefore did not use a spherical transfer code. The derived planar geometry naturally follows from a decrease in gravity by a factor of 10^4 and an increase in the radius by a factor of $\sim 10^{2.5}$ as one proceeds from the Sun to the most luminous supergiant, α Ori. Thus the ratio of pressure scale height to radius is a factor of $10^{1.5}$ larger in α Ori than in the Sun. If the chromospheres of both stars have similar temperatures and extend over a similar number of pressure scale heights, then the ratio of chromosphere thickness to radius in α Ori is $10^{1.5}$ that of the Sun, which itself is about 10^{-3}. Thus the α Ori chromosphere would be planar. However, if the momentum input by waves is large, this result may not be valid (Hartmann and MacGregor 1980). Also, there is considerable observational evidence that the chromosphere is extended (see discussion in § Vc).

After the original models for this paper were computed, the referee brought to our attention inconsistencies in the tabulated output. Subsequent checking led to the identification of errors in the computer codes[4] and a recomputation of all models and emergent line profiles. We felt that the recomputed profiles for β Dra and ϵ Gem are close enough to the observed profiles that the original temperature distributions, but with revised densities, are adequate to explain the data without further modeling. The original temperature distribution for α Ori, however, was not adequate, and the two new models discussed below were computed.

[4] With the revised computer codes we have reexamined previously published models of ϵ Eri (Simon, Kelch, and Linsky 1980) and the RS CVn systems, UX Ari and HR 1099 (Simon and Linsky 1980), and find no differences in the hydrogen ionization equilibrium or densities larger than 25% throughout the model.

IV. CHROMOSPHERIC MODELS FOR SPECIFIC STARS

The adopted stellar parameters and sources for these data are summarized in Table 5.

a) β Draconis

i) *Lower Chromosphere Model*

Our adopted static model for β Dra (see Table 6) has a relatively flat $T(m)$ distribution (see Fig. 3) in the low chromosphere with temperatures mostly near 5000 K, followed by a steep rise beginning at $m = 10^{-2}$ g cm^{-2}. The lower chromosphere portion of the model ($T < 6000$ K) was derived by matching computed and observed emission peaks and wings of the K and k lines. We found that the point at which the temperature falls below 6000 K must be within a factor of 2 of $m = 10^{-2}$ g cm^{-2} to produce a good compromise to the K- and k-line fluxes; smaller values lead to k-line fluxes that are too small, and larger values lead to K-line fluxes that are too large. The value of the temperature near $m = 1$ g cm^{-2} is very important because this region of the model has the largest effect on the profiles. Calculated profiles in Figure 4 for the sample model in Figure 3 demonstrate this effect; the peak and shoulder of the k feature seems to require temperatures near 5400 K, whereas the K_2 peak is best matched by 4900 K. Our adopted temperature at $m = 1$ g cm^{-2} is thus a good compromise.

The temperature minimum is set at 4800 K and $m = 8$ g cm^{-2}. This location could be changed by $\pm 50\%$ in m and decreased by 300 K in T without causing great mismatches to occur in the fits, particularly for Mg II. This is due to decoupling of the line wings from local

TABLE 5

ADOPTED AND DERIVED STELLAR PARAMETERS

Adopted Parameters	β Dra	ϵ Gem	α Ori
Spectral Type	G2 II	G8 Ib	M2 Iab
$T_{\rm eff}$ (K)	5375[a]	4600[a]	3150[b]
log g	1.35[a]	0.85[a]	0.0[b]
Ang. diameter (milli-arcsec)	3.27[c]	5.19[c]	54.08[c]
F(K) (ergs cm^{-2} s^{-1})	1.9(6)[d]	2.2(5)[d]	...
$F(k)$ (ergs cm^{-2} s^{-1})	1.5(6)[e]	2.8(5)[e]	1.4(4)[e]
Derived Parameters			
$T_{\rm min}$ (K)	4800	3400	2700
$m(T_{\rm min})$ (g cm^{-2})	8.0	3.3	4.3
$T_{\rm max}$ (K)	...	6500 ± 500	7000
m_0 (g cm^{-2})	5(−4)	...	...

[a] Luck 1977.
[b] Sanner 1976.
[c] Using Barnes-Evans relation. See Tables 2 and 3.
[d] Linsky *et al.* 1979*b*.
[e] Basri and Linsky 1979.

TABLE 6

MODEL FOR β DRACONIS

m (g cm^{-2})	T (K)	ρ (g cm^{-3})	n_e (cm^{-3})	n_H (cm^{-3})	v_T (km s^{-1})	z (cm)	b_1
5.0(−4)	1.6(4)	4.8(−15)	2.2(9)	2.0(9)	10	3.75(11)	9.6(5)
5.9(−4)	1.42(4)	5.6(−15)	2.6(9)	2.4(9)	10	3.67(11)	2.3(5)
7.9(−4)	1.16(4)	8.8(−15)	4.0(9)	3.7(9)	10	3.41(11)	1.3(4)
1.0(−3)	9.0(3)	1.4(−14)	5.6(9)	6.1(9)	10	3.20(11)	3.6(2)
1.4(−3)	8.4(3)	2.1(−14)	8.4(9)	9.1(9)	9.6	2.99(11)	8.7(1)
2.0(−3)	7.8(3)	3.4(−14)	1.2(10)	1.4(10)	9.3	2.76(11)	4.0(1)
2.8(−3)	7.25(3)	5.5(−14)	1.3(10)	2.3(10)	8.9	2.58(11)	2.9(1)
3.9(−3)	6.67(3)	9.3(−14)	1.1(10)	3.9(10)	8.6	2.43(11)	1.7(1)
5.6(−3)	6.09(3)	1.7(−13)	7.0(9)	7.0(10)	8.2	2.28(11)	9.1
9.7(−3)	5.7(3)	3.5(−13)	5.2(9)	1.5(11)	7.8	2.08(11)	5.4
2.6(−2)	5.57(3)	9.4(−13)	6.8(9)	4.0(11)	7.2	1.81(11)	4.3
7.0(−2)	5.48(3)	2.6(−12)	9.7(9)	1.1(12)	6.9	1.54(11)	3.7
1.86(−1)	5.4(3)	7.3(−12)	1.4(10)	3.1(12)	6.5	1.30(11)	3.3
5.0(−1)	5.3(3)	2.1(−11)	2.0(10)	8.9(12)	6.0	1.06(11)	2.7
1.25	5.1(3)	5.6(−11)	2.2(11)	2.4(13)	5.7	8.47(10)	2.0
3.27	4.97(3)	1.6(−10)	2.9(10)	6.6(13)	5.3	6.41(10)	1.6
8.0	4.8(3)	4.1(−10)	4.0(10)	1.7(14)	5.0	4.61(10)	9.6(−1)
1.5(1)	4.9(3)	7.9(−10)	7.7(10)	3.4(14)	4.5	3.40(10)	1.0
2.8(1)	5.0(3)	1.5(−9)	1.5(11)	6.5(14)	4.0	2.24(10)	1.0
6.6(1)	5.1(3)	3.8(−9)	3.3(11)	1.6(15)	3.3	7.18(9)	1.0
1.0(2)	5.2(3)	5.8(−9)	5.5(11)	2.5(15)	3.0	...	1.0

conditions as a result of their almost complete coherence as discussed by Basri (1980). Since each portion of the line profile is influenced by conditions throughout the atmosphere, the model chromosphere should not be viewed as a unique determination of the local $T(m)$ distribution required to match observations. Only by the use of both lines can we begin to narrow the range of acceptable chromospheric temperature distributions. The analysis of further diagnostic lines such as Si II, O I, and Lyα and Hα may improve the uniqueness situation, but even in the Sun it has not yet been possible to make a one-component model that is consistent with all of these diagnostics. Also, if the Sun is any guide, then the stellar surface is very inhomogeneous and should be represented by a whole set of different models averaged in some unknown fashion.

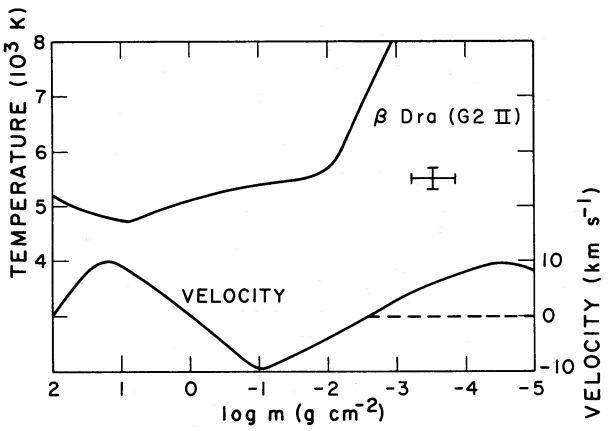

FIG. 3.—The adopted temperature-mass column density distribution for β Dra. Error bars are given to indicate roughly the degree of uncertainty in T and m resulting from the method of analysis and observational uncertainties. The bottom curve shows two systematic velocity models which were fairly successful in reproducing line profile asymmetries for β Dra.

Experience has also shown (Heasley and Milkey 1976; Ayres and Linsky 1976; Vernazza, Avrett, and Loeser 1976) that Ca II and Mg II seem to lead to hotter chromospheric models than some other diagnostics. If the incoherence fraction were larger, the observed fluxes could be matched by lower temperatures, but even in β Dra the chromospheric densities are low enough that redistribution arises mainly from radiation in other transitions. For β Dra we have computed incoherence fractions as described above, but for the more luminous stars we have considered alternatives. What is more plausible, however, is that the Mg II and Ca II lines are formed mainly in hotter, high-pressure regions in the star than the continuum, as is the case with the solar chromospheric network. It is entirely possible that our models refer only to high-field regions and not to the average stellar surface at all. For the present, however, we consider only one-component models as a first approximation since so little is known about supergiant chromospheres.

The microturbulent velocity distribution required to reproduce the emission width is determined only in the sense that velocities between 5 and 10 km s^{-1} seem to be required just above the temperature minimum. There is no need for velocities higher than that in the upper chromosphere, and they could be lower in the photosphere. The Mg II and Ca II lines cannot provide this information. Such velocities are in agreement with other determinations for supergiants such as those of Castley (1973), Böhm-Vitense (1972), or Boesgaard and Hagen (1979). High-resolution spectra of transition-region lines, like C II, would better serve to fix microturbulent velocities at the top of the chromosphere. The final mdel for β Dra and its line profiles are summarized in Figure 4 and in Table 6.

ii) *Systematic Velocity Fields*

Two striking features of the K-line profile in β Dra are the shallow central reversal and strong asymmetry, with the blue K_2 peak far brighter than the red K_2 peak. The k line shows a deep reversal and a much weaker asymmetry in the same sense. All the computed models show deep reversals for both lines, and experience with test models having different values of m_0 showed that the k reversal tends to fill in before K as one increases the pressure at the top of the atmosphere. The results of Basri (1980) indicate that a mesoscale velocity field could remove these discrepancies, but might also fill in the k-line reversal.

A variety of velocity fields were tested with the basic idea that there might be a negative velocity gradient (inflow) in the lower chromosphere but much weaker inflow velocities higher in the chromosphere, where the

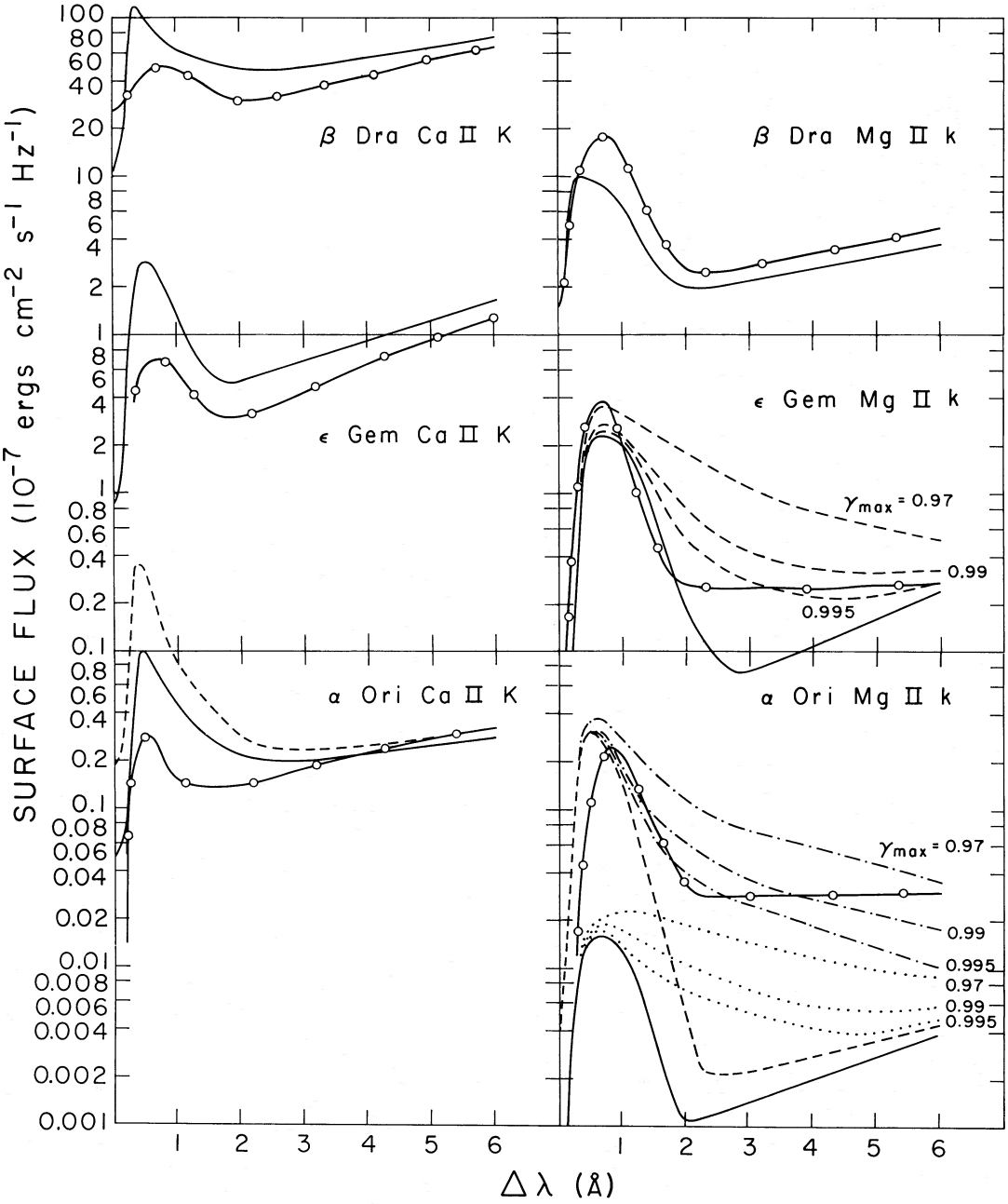

FIG. 4.—The observed (*solid line with circles*) and computed Ca II K and Mg II k line profiles for the β Dra model of Fig. 3 with no systematic velocity fields, the ϵ Gem model in Fig. 6, and the two α Ori models in Fig. 6. Also given for ϵ Gem and α Ori are computed Mg II k line profiles in which γ_{max} has been set to 0.97, 0.99, and 0.995. For α Ori the dot curves refer to the adopted (*solid line*) temperature distribution and the dash-dot curves refer to the alternative (*dashed line*) temperature distribution.

k-line core is formed. As a check, we tested the type of velocity field used by Chiu *et al.* (1977) to explain the profile asymmetry in α Boo. This flow conserves vertical mass flux, so its greatest amplitude occurs where the density is lowest at the top of the atmosphere. For this flow model, no reasonable velocity amplitude at the top of the chromosphere produces inflow velocities of sufficient amplitude at the base of the chromosphere to yield the observed Ca II asymmetry. This flow model also produces a far greater asymmetry in Mg II than Ca II, contrary to observations. Thus the flow in β Dra must be some kind of wave or circulation cell in the atmosphere which does not conserve vertical mass flux locally.

The simplest scheme that had good success in matching the observed profiles is a sinusoidal variation of vertical velocity amplitude with various wavelengths and phases. Two trial flows and resulting profiles are shown in Figures 3 and 5. These computations were unfortunately done with an earlier chromospheric model for β Dra, but our conclusions are not affected. The wave that best explains the K-line asymmetry has a wavelength of two-thirds of the atmospheric height, corresponding to 2×10^6 km. The phase is such that a velocity maximum occurs near the temperature minimum, and a velocity minimum occurs near $m = 10^{-2}$ g cm^{-2}. This is by no means a unique solution to the problem, although changes of 50% in the wavelength or $\pi/2$ in phase are definitely unsatisfactory. This particular wave, if real, is not a sound wave, as the period would be 10 times the acoustic cutoff period. Of course, there is no reason to require a sine wave, as the essential feature of the flow is the velocity gradient in the line-formation region (cf. Athay 1970; Cram 1972).

This sine wave flow explains all aspects of the K-line profiles including the relative intensities of the peaks, the shallow central reversal, and the fact that the K_{1v} flux appears to be larger than K_{1r}. It also broadens the Mg II emission feature, in better agreement with observations, preserves the deep central reversal, and narrows the central reversal feature in better agreement with the data (see Fig. 5). There is a tendency for the violet shoulder of k to be too broad, but this could be removed by shortening the wavelength of the flow slightly. A test calculation without any microturbulence produced an emission width much narrower than observed, so a microturbulent velocity distribution similar to that in the final model (see Table 6) is needed.

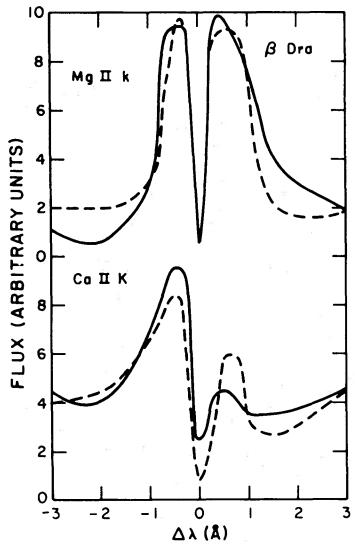

FIG. 5.—The computed line profiles for β Dra for the two velocity models of Fig. 3. Note that the central reversal in Ca II K is much shallower than for the case with no velocity field.

The physical correspondence of the flow to convection or long-period waves is not clear. The main difficulty with waves is to explain why the opposite phase, which would tend to symmetrize the K-line profile, is also not present in the chromosphere. A convection model which has the same general gradient also yields profiles which agree with observations. The dashed velocity model in Figure 3 could represent the projected downward velocity components in a convection cell. The top of the cell is in the mid-chromosphere, and the flow accelerates to a constant value in the photosphere. To explain the rather high downflow velocities, the upwelling regions must have much greater area and slower velocities than the downflowing regions. Very little is known about the behavior of convective patterns as gravity and temperature decrease from solar values, except that Schwarzschild (1975) has suggested that convection cells become much larger as gravity decreases. Vertical mass flux could be conserved in this model by a two-component atmosphere in which the upward flow in the chromosphere is cooler or has lower densities and hence weaker emission. The combination of rapid downflows (presumably at bright solar-type supergranulation cell boundaries) with slow upflows in darker supergranulation cell interiors should result in a net flux profile with an asymmetry indicating downflow. It should be noted that the β Dra K-line profile is unusually asymmetric. The λ8542 line of Ca II is also unusually shallow (Linsky *et al.* 1979*a*), and the velocity fields proposed do produce this effect.

iii) *Upper Chromosphere Model*

The portion of the β Dra model for $T > 6000$ K is much less certain than the lower chromosphere. In deriving the upper chromosphere model, we matched computed and observed values of the k-line central intensity and C II $\lambda\lambda$1334, 1335 resonance line flux, but both diagnostics are not unique. The central (minimum) intensity of the k line is sensitive to the location in mass column density of the steep temperature rise beginning near 6000 K. In our initial models we placed the beginning of this steep rise at $m = 10^{-2}$ g cm^{-2}, but these models resulted in k-line central minimum intensities brighter than observed. Moving the location of the steep temperature rise outward to $m = 10^{-4}$ g cm^{-2} produced good agreement of computed and observed central intensities. Baliunas *et al.* (1979) have proposed that for active chromosphere stars like λ And and α Aur high transition-region pressures are consistent with Ca II and Mg II fluxes, if chromospheric temperatures are reduced. One consequence of this model is to raise the core fluxes of the

TABLE 7

DENSITY-DIAGNOSTIC LINE RATIOS

Diagnostic Lines	Flux Ratio	n_e (cm^{-3})	$n_e T$[a] (K cm^{-3})	$P_0 = 2 n_e kT$ (dynes cm^{-2})
C III λ1909/Si IV λ1403	1.7[b]	1.8(10)[c]	1.1(15)	0.30
	...	1.2(10)[d]	7.2(14)	0.20
C III λ1909/O III λ1666	2.0	2.9(10)[d]	1.7(15)	0.48
C III λ1909/Si III λ1892	0.63	6(9)[c]	2.7(14)	0.075
C III λ1175/C III λ1909	0.71	2(10)[c]	1.1(15)	0.30
Model at T = 16,000 K	...	2.7(9)	4.3(13)	0.012

[a] $T = 6 \times 10^4$ for all lines except Si III λ1892 which is uncertain (see text). We have assumed $T = 3 \times 10^4$ for C III λ1909/Si III λ1892 ratio.
[b] Assuming I(Si IV λ1403) = 0.8 × I(Si IV + O IV blend) as in the Sun.
[c] Cook and Nicolas 1979.
[d] Doschek *et al.* 1978.

Ca II and Mg II lines. However, we cannot use the core fluxes as chromospheric diagnostics at least for supergiants for the following reasons: (1) interstellar Mg II absorption can obliterate the chromospheric central reversal feature for supergiants (see Böhm-Vitense 1980); and (2) systematic velocity fields and mesoturbulence (see above) can fill in the k-line core.

In our model (Table 6) we assumed a thick plateau with T = 16,000 K beginning at $m_0 = 5 \times 10^{-4}$ g cm^{-2}, as suggested by the analysis of C II observations for the Sun (Lites, Shine, and Chipman 1978) and ϵ Eri (Simon, Kelch, and Linsky 1980). The assumption of a thick plateau at 16,000 K requires $m_0 \approx 5 \times 10^{-4}$ g cm^{-2} to be consistent with the observed C II surface flux.

Density-sensitive line ratios provide an independent check on our estimated value of $m_0 \approx 5 \times 10^{-4}$. Listed in Table 7 are values of line ratios for which Doschek *et al.* (1978) and Cook and Nicolas (1979) have published line ratio electron density curves. Also given are values of n_e and $P_0 = 2n_e kT$ derived from these ratios using the unnormalized relations of Doschek *et al.* (1978) and model atmosphere relations of Cook and Nicolas. We have assumed $T = 6 \times 10^4$ K for the formation temperature of O III, Si IV, and C III. The C III λ1909/Si III λ1892 ratio is likely a poor density diagnostic, as Si III will probably form in a 16,000 K plateau if present (see Simon, Kelch, and Linsky 1980), and charge transfer reactions have not been included for Si III in the computed line ratios (Baliunas and Butler 1980).

Given the many uncertainties inherent in the line-ratio method and uncertainties in the measured line fluxes, especially important for the blended O III λ1666 feature, these data suggest $P_0 \approx 0.3$ dynes cm^{-2}. By comparison, the model in Table 6 results in $P_0 = 0.012$ dynes cm^{-2} at 16,000 K and lower values of P_0 at higher temperatures. This discrepancy of a factor of 30 in the derived value of P_0 is likely due to two reasons. First, m_0 in the model can probably be increased significantly and still be consistent with the C II and k-line core data by decreasing the thickness of the plateau and recognizing that interstellar absorption results in the k-line core being a poor diagnostic. Second, emission at 60,000 K may be dominated by high-density magnetic flux tubes that cover a small area of the disk. The resolution of this discrepancy and the computation of a self-consistent transition-region model will be attempted in a future paper in which we model lines of C II–IV and other transition-region lines and utilize line profile information being obtained by *IUE*.

b) ϵ *Geminorum*

The apparent absence of transition-region lines in ϵ Gem suggests that there is no need for the temperature to rise rapidly at some mass column density, which would define the "top" of the chromosphere. We therefore set $m_0 = 0$ and set the temperature equal to 6500 K at small values of m. The absence of hot lines does not prove that there is no top to the chromosphere, only that if there is a temperature rise it must occur at very small mass column density or occur only over a very limited region of the surface. It does seem safe to say that the chromospheric emission lines become optically thin high in the chromosphere because the gas density becomes small rather than because Ca^+ and Mg^+ become further ionized. The value of the temperature high in the ϵ Gem chromosphere is not well determined by the Ca II and Mg II data, except that it appears to be in the range of 6500 ± 500 K at $m = 10^{-6}$ g cm^{-2}. Temperatures outside this range lead to peak intensities and total fluxes, especially for Mg II, that are inconsistent with the data. An inflection in this model occurs at $m = 10^{-1}$ g cm^{-2}, where the temperature is close to 5500 K. Small changes in the location of the 5500 K inflection point have large effects on the width and intensity of k and K. The reason for this is that it is critical whether the chromospheric temperature gradient is sufficiently large to cause a rise in the core source functions, and there must be sufficient optical depth in the higher temperature material for the source function to respond to the chromospheric temperature rise because of the very low values of ϵ and Λ in this star. On the other hand, because Λ is much greater in Ca II than in Mg II, due to transitions in the Ca II infrared triplet lines, this coupling could not be too great or it would produce very bright K_2 peaks. The peak of the core source function is still orders of magnitude below the local Planck function.

The position and value of the temperature minimum is

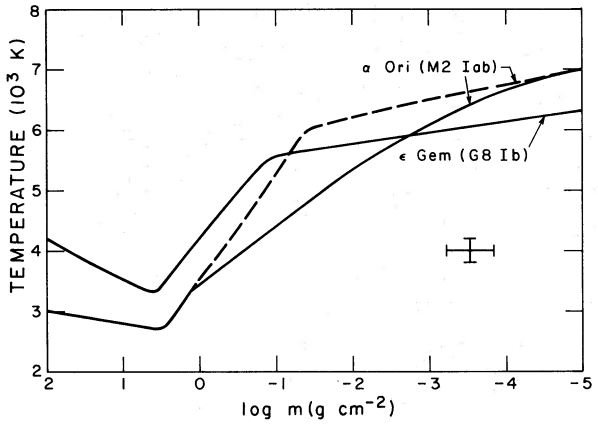

FIG. 6.—The adopted (*solid lines*) temperature and mass column density distributions for ϵ Gem and α Ori. The dashed line is an alternative model computed for α Ori.

again poorly determined, and we have adopted a minimum temperature of 3400 K. The outer wing of the K line begins to respond to local conditions because of increasing density by $m = 10^2$ g cm^{-2}, where the temperature is 4500 K. By holding down the temperature gradient above the temperature minimum, the minimum could be raised several hundred degrees. The wings of the Mg II *k* line are strongly affected by nearly coherent scattering of the background continuum. The wing intensity is sensitive to the non-LTE Balmer continuum source function which dominates the background continuum. If this source function is assumed to be in LTE, then the line wings would be far brighter than observed (cf. Basri 1980). The main conclusion that can be drawn from this analysis is that the *k* wings are not accurate local thermal diagnostics of supergiant chromospheres. The observational result of very flat wings is predicted by this model. The final model and profiles for ϵ Gem are given in Figure 6 and Table 8, and the computed profiles are shown in Figure 4.

One additional feature of the computed profiles is the deep central minima in both K and *k*. Unlike β Dra and higher gravity stars, such reversals are an observed feature in ϵ Gem. Although it is obvious that circumstellar components are present in ϵ Gem, the dark core at line center could also be intrinsic to the stellar chromosphere. The deep reversal was removed in β Dra by the addition of a large-scale velocity field, but there is less evidence for such velocities in the profiles of ϵ Gem. Because of the circumstellar components seen in other spectral lines, however, we cannot say at this time whether the deep central reversals in the Ca II and Mg II are chromospheric or circumstellar in origin.

c) α *Orionis*

The range of possible models for α Ori is similar to that for ϵ Gem. The main difference is that the temperature minimum for α Ori is reduced to 2700 K. The same comments about construction of the temperature distribution apply as for ϵ Gem, and the Ca II and Mg II lines are also most sensitive to part of the model just below $m = 10^{-1}$ g cm^{-2}. An important uncertainty in these models is a consequence of the very nonlocal nature of the line formation resulting from low values of ϵ and Λ. Since further nonuniqueness is introduced by assuming one-component models, these models are useful mostly to give a qualitative picture of the stellar chromosphere and for intercomparison with other one-component models.

We have not been able to find a single chromospheric model for α Ori that adequately fits both the Ca II and Mg II line profiles. The adopted model described in Table 9

TABLE 8

MODEL FOR ϵ GEMINORUM

m (g cm^{-2})	T (K)	ρ (g cm^{-3})	n_e (cm^{-3})	n_H (cm^{-3})	v_T (km s^{-1})	z (cm)	b_1
1.0(−6)	6.5(3)	5.0(−18)	9.0(5)	2.1(6)	13	2.31(12)	5.2(4)
2.3(−6)	6.43(3)	1.2(−17)	1.8(6)	5.2(6)	12.7	2.16(12)	2.6(4)
7.9(−6)	6.33(3)	4.5(−17)	5.4(6)	1.9(7)	12.2	1.93(12)	8.2(3)
2.75(−5)	6.23(3)	1.7(−16)	1.7(7)	7.1(7)	11.9	1.72(12)	2.0(3)
9.5(−5)	6.13(3)	6.0(−16)	5.8(7)	2.6(8)	11.5	1.52(12)	4.3(2)
3.3(−4)	6.03(3)	2.2(−15)	1.8(8)	9.3(8)	11.1	1.34(12)	1.1(2)
1.2(−3)	5.9(3)	8.7(−15)	3.9(8)	3.7(9)	10.8	1.15(12)	5.5(1)
4.2(−3)	5.81(3)	3.0(−14)	6.8(8)	1.3(10)	10.6	9.80(11)	4.6(1)
1.5(−2)	5.69(3)	1.2(−13)	1.1(9)	5.0(10)	10.4	8.08(11)	3.5(1)
5.5(−2)	5.57(3)	4.2(−13)	1.9(9)	1.8(11)	10.1	6.51(11)	2.6(1)
1.6(−1)	5.37(3)	1.3(−12)	2.4(9)	5.7(11)	9.8	5.18(11)	1.7(1)
2.9(−1)	4.98(3)	2.6(−12)	1.6(9)	1.1(12)	9.5	4.51(11)	7.9
5.3(−1)	4.52(3)	5.3(−12)	8.8(8)	2.2(12)	9.1	3.89(11)	3.4
9.8(−1)	4.2(3)	1.0(−11)	6.6(8)	4.4(12)	8.8	3.29(11)	1.8
1.8	3.82(3)	2.1(−11)	9.0(8)	8.8(12)	8.5	2.74(11)	7.3(−1)
3.3	3.50(3)	4.2(−11)	1.4(9)	1.8(13)	8.1	2.26(11)	2.6(−1)
6.3	3.49(3)	8.6(−11)	2.5(9)	3.7(13)	7.6	1.78(11)	2.5(−1)
1.3(1)	3.73(3)	1.9(−10)	6.6(9)	8.0(13)	6.9	1.27(11)	5.3(−1)
2.0(1)	3.98(3)	3.0(−10)	1.2(10)	1.3(14)	6.5	9.85(10)	8.4(−1)
5.0(1)	4.24(3)	8.3(−10)	3.5(10)	3.5(14)	5.4	4.19(10)	9.9(−1)
1.0(2)	4.5(3)	1.7(−9)	7.7(10)	7.2(14)	5.0	...	1.0

TABLE 9

MODEL FOR α ORIONIS

m (g cm^{-2})	T (K)	ρ (g cm^{-3})	n_e (cm^{-3})	n_H (cm^{-3})	v_T (km s^{-1})	z (cm)	b_1
1.0(−6)	7.0(3)	7.5(−19)	3.7(4)	3.2(5)	13	1.38(13)	4.7(7)
1.7(−6)	6.96(3)	1.3(−18)	5.7(4)	5.6(5)	12.8	1.31(13)	3.1(7)
2.8(−6)	6.9(3)	2.2(−18)	8.4(4)	9.4(5)	12.6	1.24(13)	2.0(7)
7.7(−6)	6.85(3)	6.3(−18)	1.9(5)	2.7(6)	12.4	1.12(13)	8.8(6)
1.7(−5)	6.8(3)	1.4(−17)	4.0(5)	6.1(6)	12.1	1.03(13)	4.0(6)
3.6(−5)	6.74(3)	3.1(−17)	8.1(5)	1.3(7)	11.9	9.40(12)	1.7(6)
7.7(−5)	6.64(3)	6.9(−17)	1.7(6)	2.9(7)	11.7	8.55(12)	6.0(5)
1.7(−4)	6.53(3)	1.6(−16)	3.7(6)	6.6(7)	11.5	7.69(12)	1.9(5)
3.6(−4)	6.39(3)	3.4(−16)	7.4(6)	1.4(8)	11.3	6.89(12)	5.9(4)
7.7(−4)	6.09(3)	7.6(−16)	1.4(7)	3.2(8)	11.1	6.12(12)	1.1(4)
2.1(−3)	5.90(3)	2.3(−15)	2.5(7)	9.6(8)	10.4	5.17(12)	4.2(3)
6.3(−3)	5.48(3)	7.8(−15)	2.5(7)	3.3(9)	9.5	4.25(12)	1.8(3)
1.9(−2)	5.11(3)	2.7(−14)	2.7(7)	1.1(10)	8.6	3.44(12)	8.1(2)
5.2(−2)	4.70(3)	8.8(−14)	2.9(7)	3.7(10)	7.6	2.80(12)	2.5(2)
1.15(−1)	4.42(3)	2.4(−13)	4.3(7)	9.9(10)	6.4	2.38(12)	1.2(2)
3.5(−1)	4.03(3)	8.0(−13)	5.2(7)	3.4(11)	6.0	1.88(12)	5.2(1)
1.3	3.36(3)	3.3(−12)	1.3(8)	1.4(12)	6.0	1.36(12)	1.1(1)
4.3	2.73(3)	1.3(−11)	6.5(7)	5.3(12)	5.8	9.24(11)	5.6(−1)
1.2(1)	2.82(3)	3.9(−11)	2.0(8)	1.7(13)	5.0	6.01(11)	7.2(−1)
3.5(1)	2.91(3)	1.2(−10)	5.9(8)	5.1(13)	4.6	2.88(11)	8.9(−1)
1.0(2)	3.0(3)	3.7(−10)	1.7(9)	1.5(14)	4.0	...	1.0

results in a Ca II K line profile somewhat brighter than observed but a Mg II k line profile nearly an order of magnitude too faint. These profiles are plotted as solid lines in Figure 4. On the other hand, raising the chromospheric temperatures somewhat, as shown by the dashed-line alternative temperature distributions in Figure 6, results in a good match to the Mg II k line core (dashed line in Fig. 4) but a Ca II K line profile (dashed line in Fig. 4) an order of magnitude too bright in the core. In order to explore the effects of possible additional incoherence in the k line wings, we have artificially introduced maximum values to the coherence fraction γ, by setting $\gamma_{max} = 0.97$, 0.99, and 0.995 in a manner similar to that described by Vernazza, Avrett, and Loeser (1981). The effect of decreasing the coherence (smaller values of γ_{max}) is to raise the wing intensities, but also to change the line shapes. These experiments suggest that setting $\gamma_{max} = 0.995$ is helpful in bringing better matches to the Mg II k line profiles for α Ori and also ε Gem, but smaller values of γ_{max} are unlikely.

It is clear that the presence of the temperature minimum and chromosphere are reflected only indirectly in the line profiles. This problem would be reduced somewhat for a line formed in complete redistribution (subordinate transitions are good candidates but they tend to be optically thin in the chromosphere). The strong sensitivity of the whole line profile to a narrow region of the atmosphere is another disturbing property of the solutions; it should be tested by other transfer codes to insure that it is not an artifact of the computational methods employed.

The ambiguity in interpretation of the central minimum feature in α Ori is more pronounced than for ε Gem, because there are no narrow circumstellar components seen in the Ca II and Mg II lines. The broad, flat-bottomed reversal in Ca II is easily predicted by our chromospheric model without including a circumstellar shell. This reversal could instead be circumstellar, but this possible explanation should be examined in detail using actual shell models computed with spherical radiative transfer codes. Circumstellar components are clearly seen in photospheric lines (e.g., Bernat 1977; Sanner 1976; Goldberg 1979), but since the observed Ca II and Mg II central cores can be produced without including a shell, they cannot be used to learn about a shell.

Lambert and Snell (1975) have suggested a simple isothermal chromospheric model with $T \approx 5000$ K as a possible explanation for the observed infrared excess component that cannot be accounted for by silicate dust. Assuming free-free emission from H and H^- in LTE, they derive a chromospheric pressure of ~ 6 dynes cm^{-2} for a chromospheric extent of 10^{13} cm or ~ 30 dynes cm^{-2} for a chromospheric extent of 10^{12} cm. In our model (Table 9), 10^{12} cm above the temperature minimum corresponds to $T = 4100$ K and $P = 0.3$ dynes cm^{-2}, and 10^{13} cm above the temperature minimum corresponds to $T = 6850$ K and $P = 8 \times 10^{-6}$ dynes cm^{-2}. None of these sets of parameters corresponds to their tentative model.

The α Ori models of Boesgaard and Magnan (1975) and Boesgaard and Hagen (1979), that were constructed to explain asymmetries in Fe II emission lines, were derived in a very different manner than the chromospheric models of this work. These authors did not attempt to find source functions that depend on atomic processes in Fe II (admittedly a difficult task) or to impose any conditions on the pressure equilibrium. Instead, they assumed functional forms for the source function and optical depth scales and then adjusted these parameters along with the geometry and velocity fields

until they obtained a good match to observed profiles. In the present work the chromospheric emission lines become optically thin within a few percent of the stellar radius. On the other hand, our assumption of hydrostatic equilibrium will not be valid if there is sufficient momentum flux carried by waves (Haisch, Linsky, and Basri 1980; Hartmann and MacGregor 1980). In this case, the chromosphere could be extended. Goldberg (1979) has pointed out that the central minimum velocities of chromospheric lines (D lines, Hα, and Ca II infrared triplet lines) do not share the photospheric radial velocity variations in α Ori, which suggests that the chromosphere is extended, but our experience with β Dra suggests that velocity models which would match the observations could be found in both extended and nonextended geometries. Future work should include realistic studies of Fe II and of circumstellar shells and their velocity fields, properly taking into account line formation in spherical geometries.

V. DISCUSSION

a) Energy Balance in the Chromosphere

One of the basic aims of the study of stellar chromospheres is to understand the heating sources and subsequent disposition of this energy in the outer stellar atmosphere. While it is commonly believed that the ultimate source of this energy is the turbulent motions arising from convective heat transport in the interiors of late-type stars, whether these are magnetic, acoustic, or gravity modes is the subject of debate (cf. Stein and Leibacher 1980; Ulmschneider 1979; Linsky 1980*b*). This paper does not deal with these questions directly, but we can make a few comments concerning the nature of heating and cooling in the supergiant chromospheres based on our models.

The amount of cooling that occurs in an optically thin, collisionally excited line at each depth depends on the ratio of departure coefficients for the upper and lower states of the transition and on the collisional excitation rate (cf. Athay 1976; Ayres 1981). The latter is reduced in supergiants compared to higher gravity stars because of the low electron densities, and it turns out that both K and *k* are in detailed balance throughout most of the chromosphere, except where they become optically thin near the top. The lines do not, therefore, provide much local cooling of the chromospheric plasma. It is likely that the total mechanical energy input per unit volume is less in supergiants than higher gravity stars, because the low density plasma is less able to radiate away a given input of energy, and chromospheric temperatures can reach the same value with less excess energy input. The models in this work along with earlier models for higher gravity stars serve as a good starting point for a comparative study of cooling rates (and mechanical energy input) as a function of gravity.

The low chromospheric temperature gradient is steeper in the cooler stars, but if the temperature manages to stay below that required for significant hydrogen ionization, hydrogen can effectively cool the gas to very small mass column densities. Once hydrogen is ionized, as in β Dra, the gas is thermally unstable because all of the efficient radiative cooling lines have become optically thin. The gas temperature must then rise to coronal temperatures before being able to balance the heating input. Ayres (1979) has proposed an explanation of why the low chromospheres of these low gravity stars should occur at larger mass column densities than for dwarf stars. His basic idea that the densities must be kept reasonably high to allow the gas to cool is supported by the mass column densities derived for our models. On the other hand, he has basically employed a LTE analysis, so the cooling functions for these models should be recalculated.

The three stars modeled in this paper represent a progression to lower gravity and effective temperature. Differences and similarities among the models provide some insight into the variation of line formation and chromospheric physical parameters with these stellar properties. Because all three chromospheres occur at similar temperatures and mass column densities, the number densities decrease with decreasing gravity. This leads to decreased coupling of the line source function to local conditions through decreased collisional excitation rates (lower ϵ). The amount of collisional redistribution of line-center photons to the wings also decreases, but the main source of redistribution is by radiative coupling to nearby levels. The decrease in radiation temperature along this progression of models affects this redistribution, so there is a further decoupling in the cooler stars, at least in the lower chromosphere. It is not surprising, therefore, that the integrated line surface fluxes from these chromospheres (see Table 5) decrease along this progression.

Linsky and Haisch (1979) have noted that there appears to be a dividing line in the H-R diagram between stars with and without a transition region (TR). β Dra lies very near but to the left of the dividing line, while the other two stars lie to the right. One possible explanation is that because the cool stars tend to show outflow and circumstellar features, the nonradiative energy input to the outer atmospheres of these stars goes into driving mass loss rather than into heating a TR and a corona. Our model chromospheres should be useful in detailed studies of cool star winds.

b) Velocity Fields

We wish to call attention to the importance of studying the nature of stellar velocity fields. The classical model of microturbulent broadening of spectral lines yields line profiles qualitatively different from those computed with a velocity field having the same amplitude but scale lengths comparable to photon mean-free paths (cf. Shine 1975). The most obvious effect of such "meso-velocity" fields is to fill in the line core; if these velocity fields have sufficiently long scale lengths, they can also affect the breadth and symmetry of chromospheric emission features. Unfortunately, it is impossible to gain a precise picture of the fields actually present on a stellar surface because they are spatially unresolved. Since we observe

the aggregate effect of velocities at all amplitudes, phases, and scale lengths, it is difficult to know whether the derived mean velocity field is meaningful. The interpretation of central intensities in general must take into account the possibility that there are significant effects resulting from velocity gradients which make interpretation of differences in residual intensity ambiguous.

The interpretation of line asymmetries should also be investigated further. When the red peak of K or k is brighter than the blue peak, the usual interpretation is mass outflow in the chromosphere. With the reverse asymmetry, however, it is difficult to believe that there is a strong inflow of material onto the chromosphere, especially in supergiants. The solar Mg II flux profile shows a definite "inflow" profile, yet we know there is a solar wind. One explanation is that downflows predominate in the bright supergranulation network, while upflows dominate in the darker cell interiors. A similar effect holds for solar transition region lines, which show an average downflow (Roussel-Dupre *et al.* 1976). Line asymmetries of the infall type can also be produced by gravity or acoustic waves without any bulk flows (cf. Linsky 1980*b* and references therein). It thus seems premature to interpret the reversal of asymmetries in terms of increasing mass loss without other data. Corroborating evidence for true mass outflows can come from Doppler-shifted profiles of optically thin lines, such as the circumstellar components observed in many cool supergiants.

c) *Extended Geometries*

One approximation made in this work, which should be examined more closely, is the assumption of hydrostatic equilibrium. Although turbulent pressure was included in our models, the pressure due to radiation or waves was not. Lyα radiation pressure at the top of the atmosphere is likely to exceed gravity in our cool supergiant models, similar to the case discussed by Haisch, Linsky, and Basri (1980). Also an upward flux of acoustic waves, which has been proposed as the heating mechanism for the chromosphere (e.g., Ulmschneider 1979; Stein and Leibacher 1974, 1980), or Alfvén waves will transport enough upward momentum into a supergiant chromosphere to extend its structure (Haisch, Linsky, and Basri 1980; Hartmann and MacGregor 1980). These forces mostly have the effect of increasing the geometrical extent of the upper chromosphere and lowering its densities. There is a natural feedback mechanism by which the height of the lower chromosphere will increase less than expected, however, because as the effective gravity of the star is decreased markedly by the addition of other pressure terms, densities decrease and the model chromosphere moves to deeper mass column densities in order to produce the observed line surface fluxes.

Goldberg (1979) has summarized the observational evidence for geometrical extension and mass outflow in the chromosphere of α Ori. He points out that radial velocities measured in the cores and wings of chromospheric lines, like Hα (cf. Boesgaard and Hagen 1979) and the Ca II resonance and infrared triplet lines, do not change with time, whereas photospheric lines vary over the 5.781 year period by ± 3 km s^{-1}. Thus the photosphere is physically detached from the chromosphere. Boesgaard and Magnan (1975) and Boesgaard (1979) have studied the Fe II emission lines near 3200 Å that are presumably formed at the base of the chromosphere. They find that the cores (some self-reversed) follow the radial velocity of the photosphere but are redshifted. They interpret this as infalling material extending out to 1.8 or 2.5 photospheric radii. By comparison, Goldberg (1979) shows that the wings of the Ca II infrared triplet lines have the velocity of the center of mass of α Ori, and the more opaque cores of the Ca II lines and Hα, that are found higher in the chromosphere, show Doppler shifts equal to half the expansion terminal velocity seen in circumstellar lines. Also, radio observations near 3 GHz (Altenhoff, Oster, and Wendker 1979) suggest a chromospheric extent of several photospheric radii. These data together suggest that the chromosphere extends to a few and perhaps to 10 radii, the probable inner radius of the circumstellar dust shell (cf. Castor 1981).

Since the cores of the Ca II, Mg II, and Hα lines are formed high in the chromosphere of α Ori, future models should include geometrical extension. The difficult question is how to do so in a physically self-consistent way—either by means of additional nonthermal components to the pressure or by a full dynamic calculation.

VI. CONCLUSIONS

In this paper we present and discuss observations of emission lines from chromospheres and transition regions of three supergiants and derive atmospheric models and velocity fields consistent with these data. All three stars show chromospheric emission lines of Ca II, Mg II, Si II, Fe II, C I, S I, and O I, but ϵ Gem and α Ori show no evidence for lines originating in hotter plasmas. On this basis we compute chromospheric models which extend to $m = 10^{-6}$ g cm^{-2} at temperatures rising to 6500 K (for ϵ Gem) and 7000 K (for α Ori). Upper limits on the surface flux of the C IV λ1549 emission feature in ϵ Gem are 0.1 that of the quiet Sun, and in α Ori they are 0.002 that of the quiet Sun, providing upper limits on the amount of 10^5 K plasma in the outer atmospheres of these stars. However, deeper exposures of these stars would be useful in searching for weak high-temperature emission lines. By contrast, β Dra shows strong emission features of C II–IV, Si IV, He II, and N V, indicating plasma at temperatures up to at least 2×10^5 K in the outer atmosphere of this star. We have tentatively extended the β Dra chromosphere model up to 16,000 K at $P_0 = 2n_e kT = 0.012$ dynes cm^{-2} to match the observed C II flux. However, this pressure is inconsistent with that predicted by density-diagnostic line ratios.

The property of supergiants that most sets them apart from the previously modeled dwarfs and giants is their very low gravities, which leads to lower chromospheric densities. This effect is partially offset by the larger mass column densities at which the supergiant chromospheres are apparently located. Because of the lower densities and the decreased probability of collisional destruction of

photons, radiation fields in the line cores are less thermalized. Since radiative transfer in the resonance line wings is mainly by coherent scattering as a result of decreased collisional redistribution, the wings are also only weakly coupled to local properties. Models derived from resonance line diagnostics therefore have less precision than for higher gravity cases, but the models are still valuable as the first attempts at chromospheric models in this part of the H-R diagram.

Velocity fields play an important part in the formation of spectral line profiles. We find that "meso-velocity" fields, that is, nonthermal velocities with scale lengths comparable to photon mean-free paths, can fill in line cores and affect the breadth and symmetry of chromospheric line profiles. The Ca II resonance lines in β Dra are extremely asymmetric in that the blue emission peaks are far brighter than the red peaks. Assuming homogeneous, mass flux conservative atmospheres, these lines predict a strong antiwind (mass infall) and even more asymmetric Mg II lines, contrary to observations. We show that the Ca II and Mg II lines can be simply, but not uniquely, explained by a sinusoidal meso-velocity field of large wavelength in which maximum outward velocity occurs near the temperature minimum and maximum inward velocity occurs near $m = 10^{-2}$ g cm^{-2} for a one-component atmosphere, but they could be consistent with the network component of a solar supergranulation—like the flow pattern in which bright regions (network) are downflows and dark regions (cells) are upflows in the chromosphere. Alternative physical explanations for this derived velocity field may involve acoustic or gravity waves. Further studies involving physically self-consistent flow patterns are clearly needed.

Two immediate needs for future work with supergiant model chromospheres are a better treatment of the non-LTE nature of the background continuum and metal ionization (cf. Auman and Woodrow 1975) and the analysis of other diagnostics, such as the infrared triplet of Ca II, Hα, Si II, C I, O I, and S I. These will be useful in validating the work done to date and in extending the range of the models computed. A difficult but important problem is to include possible geometric extension of supergiant chromospheres in a physically self-consistent manner. Another very interesting area of study is the atmosphere between the chromosphere and the overlying circumstellar envelope. The methods of calculating line profiles employed in this work should also be applied to the analysis of circumstellar shells themselves. Our model chromospheres, and related observations, will allow the ionization equilibrium to be evaluated with greater confidence than in the past. A wider range of stars should also be studied to better evaluate the variation of physical parameters with gravity and effective temperature. Eventually, we hope to answer some fundamental questions about the heating of chromospheres, the presence or absence of coronae, and the cause and rates of mass loss in late-type supergiants.

This work was supported in part by the National Aeronautics and Space Administration grants NAS5-23274 and NGL-06-003-057 to the University of Colorado. We wish to thank Dr. A. Boggess and the staff of the *IUE* Observatory for their assistance in the acquisition and reduction of these data, and the National Center for Atmospheric Research, operated by the University Corporation for Atmospheric Research under contract with the National Science Foundation, for a generous allocation of computer time. We also wish to thank Mr. N. Marstad for the reduction and calibration of the *IUE* data using the corrected ITF for the SWP camera. The computer codes we are now using are adaptations of NCAR CRAY-1 codes written by B. Lites and A. Skumanich, which in turn are based on codes written by R. Shine on the basis of the LINEAR-A code written by J. Heasley, D. Mihalas, and R. Milkey, and the Rybicki method of solving the transfer equations first coded by J. Heasley and L. Auer. We wish to thank these people and E. Avrett for pointing out errors in the computed models, and B. Lites and A. Skumanich for help in correcting the codes.

REFERENCES

Altenhoff, W. J., Oster, L., and Wendker, H. J. 1979, *Astr. Ap.*, **73**, L21.
Athay, R. G. 1970, *Solar Phys.*, **11**, 347.
———. 1976, *The Solar Chromosphere and Corona: Quiet Sun* (Boston: Reidel).
Auman, J. R., and Woodrow, J. E. J. 1975, *Ap. J.*, **197**, 163.
Ayres, T. R. 1975, Ph.D. thesis, University of Colorado.
———. 1977, *Ap. J.*, **213**, 296.
———. 1979, *Ap. J.*, **228**, 509.
———. 1981, *Ap. J.*, **244**, 1064.
Ayres, T. R., and Linsky, J. L. 1976, *Ap. J.*, **205**, 874.
———. 1980, *Ap. J.*, **241**, 279.
Ayres, T. R., Moos, H. W., and Linsky, J. L. 1981, *Ap. J.* (*Letters*), **248**, L137.
Baliunas, S. L., Avrett, E. H., Hartmann, L. W., and Dupree, A. K. 1979, *Ap. J.* (*Letters*), **233**, L129.
Baliunas, S. L., and Butler, S. E. 1980, *Ap. J.* (*Letters*), **235**, L45.
Basri, G. S. 1980, *Ap. J.*, **242**, 1133.
Basri, G. S., and Linsky, J. L. 1979, *Ap. J.*, **234**, 1023.
Basri, G. S., Linsky, J. L., Bartoe, J.-D. F., Brueckner, G. E., and van Hoosier, M. C. 1979, *Ap. J.*, **230**, 924.
Bernat, A. P. 1977, *Ap. J.*, **213**, 756.
Bernat, A. P., and Lambert, D. L. 1976, *Ap. J.*, **204**, 803.
Boesgaard, A. M. 1979, *Ap. J.*, **232**, 485.
Boesgaard, A. M., and Hagen, W. 1979, *Ap. J.*, **231**, 128.
Boesgaard, A. M., and Magnan, C. 1975, *Ap. J.*, **198**, 369.
Boggess, A. *et al.* 1978, *Nature*, **275**, 377.
Böhm-Vitense, E. 1972, *Astr. Ap.*, **17**, 335.
———. 1980, preprint.
Burton, W. H., and Ridgeley, A. 1970, *Solar Phys.*, **14**, 3.
Carpenter, K. G., and Wing, R. F. 1979, *Bull. A.A.S.*, **11**, 419.
Cassatella, A., Holm, A., Ponz, D., and Schiffer, F. H. 1980, *NASA IUE Newsletter*, No. 8, p. 1.
Castley, J. 1973, *Astr. Soc. Australia Proc.*, **2**, 200.
Castor, J. 1981, in *Physical Processes in Red Giants*, ed. I. Iben, Jr. and A. Renzini (Boston: Reidel), p. 285.
Chiu, H. Y., Adams, P. S., Linsky, J. L., Basri, G. S., Maran, D. P., and Hobbs, R. W. 1977, *Ap. J.*, **211**, 453.
Cohen, L., Feldman, U., and Doschek, G. A. 1978, *Ap. J. Suppl.*, **37**, 393.
Cook, J. W., and Nicolas, K. R. 1979, *Ap. J.*, **229**, 1163.
Cram, L. E. 1972, *Solar Phys.*, **22**, 375.

de Jager, C., Kondo, Y., Hoekstra, R., van der Hucht, K. A., Kamperman, T. M., Lamers, H. J. G. L. M., Modisette, J. L., and Morgan, T. H. 1979, *Ap. J.*, **178,** 495.
Doschek, G. A., Feldman, U., Bhatia, A. K., and Mason, H. E. 1978, *Ap. J.*, **226**, 1129.
Goldberg, L. 1979, *Quart. J.R.A.S.*, **20**, 361.
Haisch, B. M., Linsky, J. L., and Basri, G. S. 1980, *Ap. J.*, **235,** 519.
Haisch, B. M., Linsky, J. L., Weinstein, A., and Shine, R. A. 1977, *Ap. J.*, **214**, 785.
Hartmann, L., Dupree, A. K., and Raymond, J. C. 1980, *Ap. J. (Letters)*, **236**, L143.
Hartmann, L., and MacGregor, K. B. 1980, *Ap. J.*, **242**, 260.
Heasley, J. N., and Milkey, R. W. 1976, *Ap. J. (Letters)*, **205**, L43.
Kelch, W. L., and Linsky, J. L. 1978, *Solar Phys.*, **58**, 37.
Kelch, W. L., Linsky, J. L., Basri, G. S., Chiu, H. Y., Chang, S., Maran, S. P., and Furenlid, I. 1978, *Ap. J.*, **220,** 962.
Kelch, W. L., Linsky, J. L., and Worden, S. P. 1979, *Ap. J.*, **229**, 700.
Lambert, D. L., and Snell, R. L. 1975, *M.N.R.A.S.*, **172**, 277.
Linsky, J. L. 1980*a*, in *Stellar Turbulence*, ed. D. F. Gray and J. L. Linsky (New York: Springer), p. 248.
———. 1980*b*, *Ann. Rev. Astr. Ap.*, **18**, 439.
———. 1981, in *Physical Processes in Red Giants*, ed. I. Iben, Jr. and A. Renzini (Boston: Reidel), p. 247.
Linsky, J. L., and Haisch, B. M. 1979, *Ap. J. (Letters)*, **229,** L27.
Linsky, J. L., Hunten, D. M., Sowell, R., Glackin, D. L., and Kelch, W. L. 1979*a*, *Ap. J. Suppl.*, **41**, 481.
Linsky, J. L., Worden, S. P., McClintock, W., and Robertson, R. M. 1979*b*, *Ap. J. Suppl.*, **41**, 47.
Linsky, J. L. *et al.* 1978, *Nature*, **275**, 389.
Lites, B. W., Shine, R. A., and Chipman, E. G. 1978, *Ap. J.*, **222**, 333.
Luck, R. E. 1977, *Ap. J.*, **218**, 752.
Roussel-Dupre, D. C., Shine, R. A., Chipman, E. G., Bruner, E. C., Lites, B. W., Rottman, G. J., and Orall, F. Q. 1976, *Bull. A.A.S.*, **8**, 312.
Sanner, F. 1976, *Ap. J. Suppl.*, **32**, 115.
Schwarzschild, M. 1975, *Ap. J.*, **195**, 137.
Shine, R. A. 1975, *Ap. J.*, **202**, 543.
Shine, R. A., and Linsky, J. L. 1974, *Solar Phys.*, **39**, 49.
Shine, R. A., Milkey, R. W., and Mihalas, D. 1975, *Ap. J.*, **199,** 724.
Simon, T. Kelch, W. L., and Linsky, J. L., 1980, *Ap. J.*, **237,** 72.
Simon, T., and Linsky, J. L. 1980, *Ap. J.*, **241,** 759.
Stein, R. F., and Leibacher, J. 1974, *Ann. Rev. Astr. Ap.*, **12,** 407.
———. 1980, in *Stellar Turbulence*, ed. D. F. Gray and J. L. Linsky (New York: Springer), p. 225.
Stencel, R. E. 1978, *Ap. J. (Letters)*, **223,** L37.
Stencel, R. E., and Mullan, D. J. 1980, *Ap. J.*, **238**, 221.
Turnrose, B., Bohlin, R., and Harvel, C. 1980, *NASA IUE Newsletter*, No. 8, p. 28.
Uesugi, A., and Fukuda, I. 1970, *Contr. Inst. Astr. Kwasan Univ.*, **33**, 205.
Ulmschneider, P. 1979, *Space Sci. Rev.*, **24**, 71.
Vernazza, J. E., Avrett, E. H., and Loeser, R. 1976, *Ap. J. Suppl.*, **30**, 1.
———. 1981, *Ap. J. Suppl.*, **45,** 635.
Wilson, O. C., and Bappu, M. K. V. 1957, *Ap. J.*, **125**, 661.

Note added in proof.—D. L. Lambert has brought to our attention that a line of Fe I multiplet UV 3 at 2803.169 Å lies near the red peak of the Mg II *h* line in α Ori. If this Fe I line is a significant circumstellar absorber, then the absence of *h* line asymmetry would be consistent with the high mass loss rate. We do not believe that the Fe I λ2803.169 line is a significant absorber of the *h* line red peak, since there is no detectable fluorescence emission at larger wavelengths produced either by this line or the stronger λ2795.006 line in the same multiplet, which lies at the blue peak of the Mg II *k* line. By contrast, fluorescent emission lines of Fe I multiplet UV 44 at 2823 Å and 2844 Å are pumped by lines of the same multiplet at 2795.5 Å located near the dark core of the Mg II *k* line.

GIBOR S. BASRI: University of California, Space Sciences Laboratory, Grizzly Peak Boulevard, Berkeley, CA 94720

KJELL ERIKSSON: Astronomiska Observatoriet, Box 515, 75120 Uppsala, Sweden

JEFFREY L. LINSKY: Joint Institute for Laboratory Astrophysics, University of Colorado, Boulder, CO 80309